Nanoscale

Accepted Manuscript

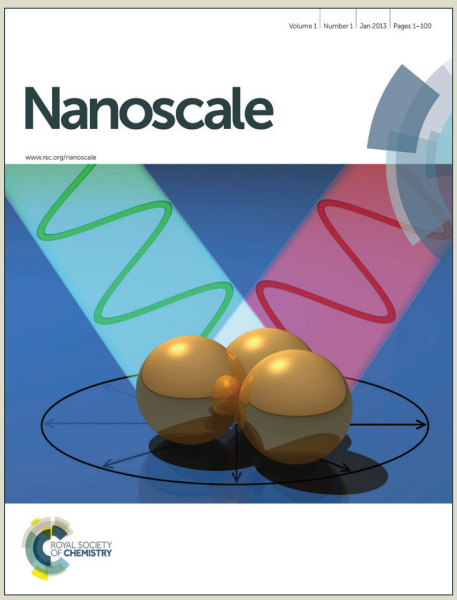

ROYAL SOCIETY OF CHEMISTRY

www.rsc.org/nanoscale

ARTICLE TYPE www. rsc.org/xxxxxx | XXXXXXXX

Conformation-dependent DNA Attraction

Weifeng Li,[a,b] Lars Nordenskiöld,[b] Ruhong Zhou,*[a,c] and Yuguang Mu*[b]

Received Xth XXXXXXXXXX 20XX, Accepted Xth XXXXXXXXX 20XX
First published on the web Xth XXXXXXXXXX 200X
DOI: 10.1039/b000000x

Understanding how DNA molecules interact with other biomolecules is related to how they utilize their functions and is therefore critical for understanding their structure-function relationships. For a long time, the existence of Z-form DNA (a left-handed double helical version of DNA, instead of the common right-handed B-form) has puzzled the scientists, and the definitive biological significance of Z-DNA has not yet been clarified. In this study, the effects of DNA conformation in DNA-DNA interactions are explored by molecular dynamics simulations. Using umbrella sampling, we find that for both B- and Z-form DNA, surrounding Mg^{2+} always exert themselves to screen the Coulomb repulsion between DNA phosphates, resulting in very weak attractive force. On the contrary, a tight and stable bound state is discovered for Z-DNA in the presence of Mg^{2+} or Na^{+}, benefiting from their hydrophobic nature. Based on the contact surface and a dewetting process analysis, a two-stage binding process of Z-DNA is outlined: two Z-DNA first attract each other through charge screening and Mg^{2+} bridges to phosphate groups in the same way as that of B-DNA, after which hydrophobic contacts of the deoxyribose groups are formed via a dewetting effect, resulting in stable attraction between two Z-DNA. The highlighted hydrophobic nature of Z-DNA interaction from the current study may help to understand the biological functions of Z-DNA in gene transcription.

1 Introduction

The DNA duplex has two negatively charged phosphate backbone strands spiraling around the middle core of nucleotide base pairs. Due to the high negative charge of this polyelectrolyte, the inter-DNA interaction is electrostatically repulsive without counterions. However, meters-long genomic DNA are packed by nature into compact structures for all living beings. To condense DNA, attractive forces must outstrip the repulsive forces. In most eukaryotic cell nuclei, DNA is packed by forming a complex with specialized histone proteins in the form of chromatin[1]. In phage heads and sperm, DNA packaging is mediated by simple counterions like the polyamines. Ion-mediated DNA-DNA interaction has been studied extensively. Monovalent alkali cations (Li^{+}, Na^{+}, K^{+}, Rb^{+}, Cs^{+}) hardly induce attractive forces between DNA. The situation in the presence of divalent cations is controversial and normally the common divalent cations (Ca^{2+}, Mg^{2+}) do not induce DNA condensation or exhibit DNA-DNA attraction[2,3]. However, a recent careful small angle x-ray scattering (SAXS) study by *Qiu* and co-workers conclusively demonstrated the existence of weak DNA-DNA attraction for short DNA strands in the presence of Mg^{2+} ions[4]. This attraction is normally not sufficient to induce phase separation except in low-dielectric medium solvent, which amplifies the attraction[5]. The apparent discrepancy between this result and the observation of repulsive forces in the work of *Rau* and *Parsegian*[2] may be due to the high molecular weight cell extracted DNA used in that latter work. On the other hand, the weak attraction in the presence of Mg^{2+}, demonstrated by negative second virial coefficients, was clearly observed by *Qiu* and co-workers[4], which depends on DNA oligonucleotide length (8 and 16 *bp* dsDNA), similar to our current lengths in simulations. Cations with charge +3 or higher, such as cobalt hexamine^{3+}, spermine^{3+} and spermidine^{4+} are usually required to condense DNA in a salt-dependent manner as observed in *in vitro* experiments[5–7]. Another class of DNA condensing agents comprises the transition metal ions, like Mn^{2+}, Co^{2+}, Ni^{2+} and Zn^{2+}[2,8,9]. Both analytical theories and computer simulations have been carried out to reveal the origin of like-charged DNA-DNA attraction and the roles of cations near DNA[10–17]. Generally, the DNA-DNA interaction is caused by ion fluctuations and charge-bridging effects and is cation-dependent.

Besides extensive reports of cation-dependent DNA condensation, there are increasing evidences that the formation of the left-handed Z-form DNA also plays an important role in promoting and regulating DNA condensation processes[8,9,18–20]. E.g., in sub-millimolar concentration of the Ni^{2+} electrolyte, a repeating-GC DNA sequence adopts Z-form and condenses easily[8]. On the contrary, an AT-rich DNA sequence remains as the B-form and displays very minor con-

[a] *Institute of Quantitative Biology and Medicine, School for Radiological & Interdisciplinary Sciences (RAD-X), Soochow University, Suzhou, China 215123*
[b] *School of Biological Sciences, Nanyang Technological University, Singapore 637551; E-mail: ygmu@ntu.edu.sg (Y.M.)*
[c] *Computational Biology Center, IBM Thomas J. Watson Research Center, New York, USA 10598; E-mail: ruhongz@us.ibm.com (R.Z.)*

densation even at much higher Ni^{2+} concentration (10 times higher than that used to condense GC-DNA)[8]. Moreover, by inserting 12- or 20-*bp* Z-form DNA segments into the pUC18 plasmids, the plasmids were found to undergo significantly enhanced condensation[21]. From these studies, a different interaction paradigm emerges: compared to B-DNA, Z-DNA interacts stronger with another Z-DNA or B-DNA, which promotes the condensation.

Since its discovery in 1979, the biological relevance of Z-DNA has attracted much attention[22]. The Z-conformation was believed to trap the negative supercoiling when transcription occurs[23,24]. However, the findings of the Z-DNA binding motif, $Z\alpha$ domain of the human RNA editing enzyme ADAR1[25–29] indicate a new role in gene transcription. In human genes, the potential Z-DNA forming sequences are found to accumulate at the upstream (5′) region to the transcriptional start sites (TSS)[30–33]. The correlation between Z-DNA formation and transcriptional activity observed in experiments[34–37] suggests the potential way of the Z-DNA in regulating the transcription: $Z\alpha_{ADAR1}$ selectively binds to Z-DNA segment so that ADAR1 can find the TSS. Then, a key question arises: How does the $Z\alpha_{ADAR1}$ find the Z-DNA segments which are surrounded by B-DNA?

In contrast to the extensive studies of B-DNA with both experimental and theoretical approaches, there have been few reports on the Z-DNA interactions. Some basic questions, such as what conformational factors are responsible for the biological functions of Z-DNA, and how this special genome version interacts with other biological molecules like protein and other DNA, remain poorly understood[24,38]. The lack of detailed knowledge of Z-DNA properties is becoming an obstacle for further understanding the Z-DNA structure-function relationship.

In the current study, all-atom molecular dynamics (MD) simulations were performed to explore the interactions between short (10 and 12 *bp*) DNA double helices in the presence of $MgCl_2$ electrolyte, where effects from both DNA conformation and sequence were taken into account. For B-DNA, attractive forces are observable, but the attraction strengths are weak. On the contrary, for Z-DNA, it is interesting that significantly stronger attraction (as compared to the B-form), accompanied with a tight and stable bound state is discovered, and this bound state is proved to be meta-stable even in pure Na^+ electrolyte, revealed by umbrella sampling and normal MD simulations. The strong attraction benefits from the unique structural properties of this special form of DNA: 1. the hydrophobic deoxyribose groups are exposed to the solvent, so that Z-DNA is more hydrophobic than B-DNA; 2. the negative-charged phosphate groups of one strand are partially buried which effectively weaken the Coulomb repulsion between Z-DNA molecules. As a result, two Z-DNA can form closer contact through the bridging-cations between the phosphate groups and are further stabilized by the hydrophobic contacts between the sugar groups. Based on the contact surface and a dewetting process analysis, a two-stage binding of Z-DNA is outlined: two Z-DNA first attract each other through charge screening and Mg^{2+} bridges to phosphate groups in the same way as that of B-DNA, after which hydrophobic contacts of the deoxyribose groups are formed via nanoscale dewetting, resulting in strong attraction between two Z-DNA. The highlighted hydrophobic nature of Z-DNA interaction may help to understand their biological significance in gene transcriptional regulation.

2 Methods

2.1 DNA-models

In all of the simulations, we have considered two identical DNA duplexes submerged in a simulation box with periodic boundary conditions imposed in all directions. The simulation box is a parallelogram in the *xy* plane, with a geometric angle of 60° as illustrated in Fig. 1(a). The volume of such a box is 0.866 of that of a rectangular box with the same periodic image distance in the *xy* plane. For B-DNA, the helix repeat is 10 *bp* per turn with a pitch length of 3.4 nm. Four sequences have been considered: d(5′-A_{10})·d(5′-T_{10}), d(5′-$(AT)_5$)·d(5′-$(AT)_5$), d(5′-G_{10})·d(5′-C_{10}) and d(5′-$(GC)_5$)·d(5′-$(GC)_5$). These four systems are abbreviated as AA-BDNA, AT-BDNA, GG-BDNA and GC-BDNA. The "sticky" ends mean that the 3′ end of each DNA strand is connected to the periodic image of 5′ end over the boundary (as shown in Fig. 1(b), the box length in the *z* direction is equal to the pitch length). This setup mimics two infinitely long DNA duplexes where only lateral interaction is considered[16,39]. Such model is not suitable for studies of DNA ends stacking[40] and DNA crossover[41]. The helix repeat in Z-DNA is 12 *bp* per turn with a pitch length of 4.46 nm. As resolved by experiments, Z-DNA usually forms from repeating guanine-cytosine sequences[8,21,23,42,43]. Hence we have only considered one sequence of Z-DNA model: d(5′-$(GC)_6$)·d(5′-$(GC)_6$) (abbreviated GC-ZDNA). The initial DNA structures were created with Discovery Studio[44].

2.2 Simulation details

In addition to DNA, the simulation boxes for B-DNA and Z-DNA systems contain 4300 and 6200 water molecules, respectively. 25 and 35 Mg^{2+} were added in both B-DNA and Z-DNA systems to maintain a mole fraction of $n_{Mg^{2+}}/n_{H_2O} = 0.0057$. To neutralize the system, 10 and 22 Cl^- were further added. Apart from Z-DNA in $MgCl_2$ electrolyte, a system with two Z-DNA in the presence of Na^+ was chosen as the control system, where only 48 Na^+ were added to neutralize

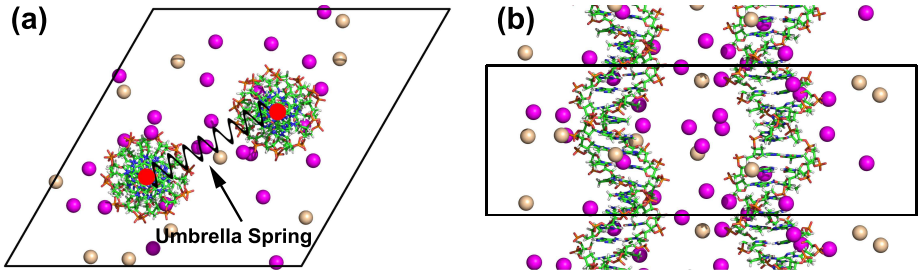

Fig. 1 Illustration of the simulation box **(a)** top view and **(b)** side view. Fig. **(a)** also demonstrates how two DNA are connected by a spring through centers of mass (shown as red balls) in the umbrella sampling simulation.

the DNA charge.

The choice of Mg^{2+} as cation is inspired by the recent experimental findings that Z-DNA can be found in both 0.7 M $MgCl_2$ [21] and mM concentration of $NiCl_2$ [8]. We chose Mg^{2+} instead of Ni^{2+} mainly because the force field parameters for Mg^{2+} are more widely used and validated[45,46], while parameters for transition metal ions such as Ni^{2+} are much less studied.

All simulations were carried out using the GROMACS[47] package. The modified AMBER(parmbsc0) force-field[48] was used for DNA and the TIP3P water model[49] for the explicit solvent. SHAKE constraints[50] were applied to all bonds involving hydrogen atoms. For counterions, the recently refined parameters for Na^+ and Mg^{2+}-hexahydrates by *Aleksei Aksimentiev* and coworkers were used[51]. The long-range electrostatic interactions were treated with the Particle Mesh Ewald method[52,53], and a typical distance cutoff of 12 Å was used for the van der Waals interactions. The non-bonded interaction pair-list was updated every 10 fs. Constant-pressure, constant-temperature (1 atm and 300 K) molecular dynamics with a movement integration step of 2 fs was used for each system.

To overcome the weakness of normal MD, one can resort to advanced sampling techniques, such as replica-exchange molecular dynamics, meta-dynamics, umbrella sampling, etc. For the currently studied system, the inter-DNA distance is a principle variable that efficiently describes the DNA – DNA interaction. In this study, the potential of mean force (PMF) profiling with respect to inter-DNA distance was first conducted with the umbrella sampling method[54]. Two DNA molecules were fully free except that the inter-DNA distance (measured by the center of mass, COM) in the *xy* plane was restrained with a harmonic spring as illustrated in Fig. 1(a). The inter-DNA distance was sampled from 1.90 nm (for B-DNA) and 1.60 nm (for Z-DNA) to 3.60 nm with a resolution of 0.05 nm. Normally, a force constant of 1000 kJ/(mol · nm^2) was used. For the consideration of strong interaction between two Z-DNA from 1.75 nm to 2.10 nm, a higher sampling resolution of 0.025 nm and a stronger force constant (2000 kJ/(mol · nm^2)) were used. At each distance, the system was first equilibrated for 10 ns followed by a 100 ns productive simulation. Statistical uncertainties were estimated using the technique of bootstrap analysis[55].

After umbrella sampling simulations, normal MD simulations for GC-BDNA with Mg^{2+}, GC-ZDNA with Mg^{2+}, GC-ZDNA with Na^+ were further performed, beginning from the dissociated state (at a distance of 3.2 nm) and the bound state (corresponding to the global minimum of the PMF profiles) for each case. Each simulation was conducted for 300 ns.

2.3 The analysis of DNA structure

The DNA structural features (including Fig. 4 and Table 1) were analyzed from the simulations where two DNA were separated at 3.5 nm (treated as fully non-interacting).

3 Results and discussion

3.1 Potential of mean force

The PMFs for the case of B-DNA are summarized in Fig. 2(a). For the case of GG-BDNA, the PMF is flat with no obvious local minima. For AA- and GC-BDNA, the PMF has one and two local minima respectively, where the depth never exceeds -0.4 kcal/mol. AT-BDNA has the lowest attractive potential well with a depth of -0.62 kcal/mol at 2.41 nm. Overall, a sharp increase is observed (except GC-BDNA) at about 2.4 nm which is caused by the steric hindrance of DNA surface. The inter-DNA distance is close to the experimental estimation observed in the presence of Mn^{2+} ions[2]. A simulation study of an array of 64 parallel duplex DNA in aqueous solution and under osmotic pressure, employing the same force field gave an average inter-DNA distance of 2.9 nm[51]. The discrepancies between our prediction and this data may be due to the DNA pair model used in the current paper. The attractive potential well of B-DNA is shallow and thus not expected to be able to lead to DNA condensation. Such a weak DNA–DNA attraction is in agreement with the observations obtained

from SAXS in the study by *Qiu* and co-workers[4]. On the contrary, the osmotic pressure data by *Rau* and *Parsegian*[2] displayed rather strong repulsion in the presence of Mg^{2+}. The present study was conducted for 10 *bp* DNA, which is similar to the 8 and 16 *bp* in the SAXS study of *Qiu* and co-workers[4], who found a strong dependence on DNA length in the observed second virial coefficients. We suspect that the major origin of the discrepancy between our simulation results and *Rau* and *Parsegian*'s experimental data[2] is due to the considerably longer DNA strands (with much higher molecular weight) used in their osmotic pressure experiments. For longer DNA chains the loss in configurational entropy is expected to give a significant contribution to the free energy change upon DNA condensation[56].

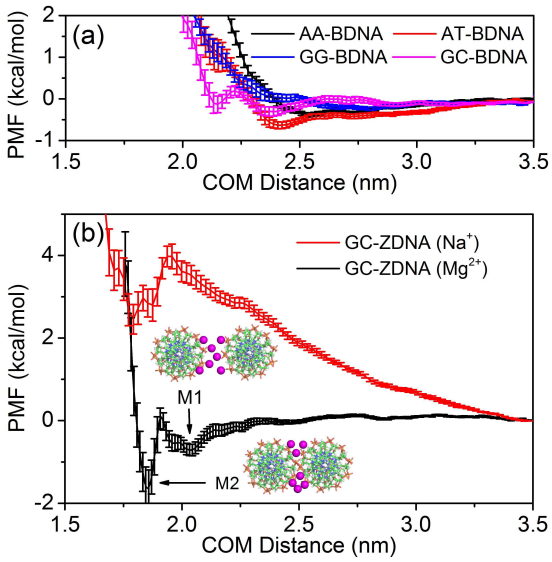

Fig. 2 Potentials of mean force (PMF) with respect to inter-DNA distance between **(a)** two B-DNA and **(b)** two Z-DNA. Free energy values at 3.5 nm are set to 0. The cartoons in Fig. **(b)** illustrate the binding pattern and positions of Mg^{2+}.

The PMFs for Z-DNA are distinct from those of B-DNA as shown in Fig. 2(b). In Mg^{2+} electrolyte, the first potential well (a local minimum, labeled as M1) appears at 2.04 nm with a depth of -0.71 kcal/mol. After overcoming an energy barrier of 0.80 kcal/mol at 1.91 nm, the second potential well (the global minimum, labeled as M2) is discovered at 1.85 nm with a depth of -1.64 kcal/mol. The smaller inter – Z-DNA distance of the M2 state is partially due to the smaller diameter of Z-DNA (1.8 nm), as compared to B-DNA (2.0 nm). In the control simulation of Z-DNA with Na^+, strong repulsive force is observed when the inter – Z-DNA distance is larger than 1.95 nm. This phenomenon is in agreement with the B-DNA case where monovalent alkali cations (Li^+, Na^+, K^+, Rb^+, Cs^+) can hardly induce attractive force because of weaker charge-

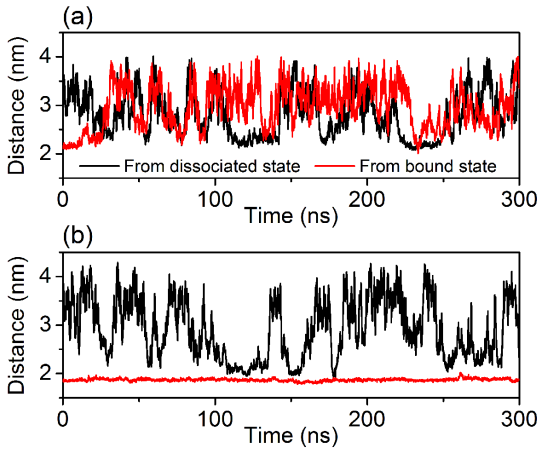

Fig. 3 Inter-DNA distance from normal simulations of **(a)** two B-DNA and **(b)** two Z-DNA in Mg^{2+} electrolyte, beginning from either dissociated state (black curve) or bound state (red curve).

screening effect than divalent cations[16]. However, it is interesting that, at 1.79 nm, a deep attractive potential well, -1.52 kcal/mol, is observed. The common feature of Z-DNA attractions in the presence of Mg^{2+} or Na^+ lies in the smaller inter – Z-DNA distance (about 1.8 nm) of the bound state. This distance is compatible to the Z-DNA diameter (also 1.8 nm). This implies that two Z-DNA have formed direct contacts, and there is short-range binding force specifically for Z-DNA.

On the contrary, the bound distances of two B-DNA are around 2.1-2.4 nm, which are larger than the B-DNA diameter (2.0 nm). Therefore, B-DNA attractions are solvent-mediated, with some water molecules in-between. This difference also indicates that Z-DNA surface is distinct from that of B-DNA.

3.2 Free DNA diffusion from normal simulations

Apart from the above umbrella sampling, normal MD simulations of two freely diffusive DNA also provide valuable information of their interactions. We have considered the situations beginning from either dissociated state or bound state, for both B-DNA and Z-DNA pairs. For the B-DNA pair as shown in Fig. 3(a), the two B-DNA are quite diffusive during the 300 ns simulations, regardless of the starting distance. The initial bound state (distance < 2.20 nm) only lasts for 10 ns, after that, the two B-DNA begin to dissociate and completely seperate around 27 ns.

Two Z-DNA beginning from the dissociated state also diffuse in a free manner as shown in Fig. 3(b), with several temporary bound states formed (corresponds to M1). However, the observed minimum value of the inter – Z-DNA distance is 1.93 nm. The two Z-DNA could not overcome the energy barrier at 1.91 nm and hence the bound state at M2 could not be accessed during the 300 ns simulation. On the contrary, when

two Z-DNA are placed in close contact in Mg^{2+} electrolyte from the start of the simulation, they can maintain the bound state stably during the 300 ns simulation. Moreover, the bound state of two Z-DNA in pure Na^{+} electrolyte is also proved to be stable during a 300 ns simulation (a movie can be found in the Electronic Supplementary Information). These results reflect the fact that the attractive force between two Z-DNA are strong, which can resist to thermal fluctuations at 300 K.

3.3 The structural features of DNA

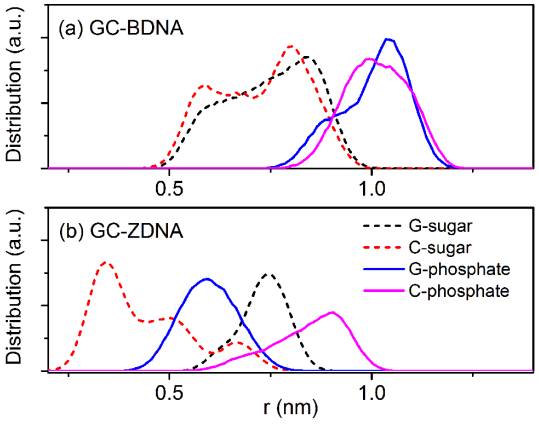

Fig. 4 Radial atomic distribution of sugar (C1′ – C5′) and phosphate groups (O1P, O2P) with respect to the center of mass in DNA axes of **(a)** GC-BDNA and **(b)** GC-ZDNA. G and C stands for nucleotides of guanine and cytosine, respectively.

The different binding behaviors between B-DNA and Z-DNA are rooted in the different features of DNA surfaces of these two conformations. Two major structural differences between B-DNA and Z-DNA are the sugar pucker and the configuration of the glycosidic bond in dG[57]. The radial atomic distributions of the ribose sugar (C1′ – C5′ carbon) and phosphate group (O1P, O2P) with respect to the center of mass in DNA axes are shown in Fig. 4. For B-DNA, all sugar residues exist in the C2′-endo configuration. As a result, the outermost surface is composed of phosphate atoms only, while sugar atoms are located about 0.25 nm closer to the center. While in Z-DNA, the sugar pucker for dC remains C2′-endo, but the pucker changes to C3′-endo in dG residues. This dissimilarity leaves only the phosphate group of dC exposed to the environment, followed by the sugar group of dG. The phosphate group of dG is buried deeper inside the double helix, which will definitely weaken the electrostatic repulsion to another Z-DNA helix, as compared to B-DNA.

A quantitative description of the DNA surface can help us to understand the structure-function relationship of the two forms of DNA. Those atoms with solvent accessible surface (SAS) larger than 0.1 nm^2 are listed in Table 1. It is obvious that the transition from B- to Z-form leaves O6 and N7 of guanine base exposed to the solvent. O6 and N7 are highly negative-charged atoms, acting as potential binding sites for cations. This is consistent with the previous findings that transition metal ions bind specifically to the N7 atom of guanine and induce the B- to Z-DNA transition, after which the N7 atom of guanine becomes more accessible[58–60].

3.4 Mg^{2+} bridges between two DNA

From previous literature, Mg^{2+} ions prefer to bind to phosphate atoms through hydrogen-bond[46]. When two DNA approaching each other, Mg^{2+} ions accumulate at the interfacial area and form hydrogen-bonds with two DNA simutaneously, like "bridges" between them. These Mg^{2+} ions exert an effective attractive force between two DNA[16,39]. The different surface, especially the negative-charged atoms, between B- and Z-form DNA would influence Mg^{2+} ions binding and, accordingly, DNA-DNA attraction. Quantitative characterizations of the Mg^{2+}-bridge network would help to quantify the contributions from these cations. In our calculation, a Mg^{2+}-bridge is regarded as formed when the distances to two DNA are simultaneously less than 0.5 nm[46]. As shown in Fig. 5(a, d), the number of Mg^{2+}-bridge (normalized to *bp*) for AT-BDNA at 2.41 nm is 0.07 per *bp*, compared to a value of only 0.05 for GC-ZDNA at M1 (2.04 nm). Less Mg^{2+}-bridges are formed between two GC-ZDNA, compared to that of two AT-BDNA. However, the value of PMF of two-ZDNA at this distance is deeper than those of B-DNA (-0.71 *.vs.* -0.62 kcal/mol). Clearly, the number of Mg^{2+}-bridge is not a solo contribution to DNA attraction. When two GC-ZDNA approach further and form direct contact at M2 (1.85 nm), the Mg^{2+} ions at the interfacial area will be squeezed out to the peripheries as illustrated in the insert of Fig. 2(b). This squeezing process corresponds to the energy barrier between M1 and M2, which is 0.8 kcal/mol. Finally, the number of Mg^{2+}-bridge reaches a value of 0.13 per *bp*. The attraction potential well is -1.64 kcal/mol (it is -1.52 kcal/mol for the Na^{+} case; it is commonly accepted that monovalent cations like Na^{+} bind to DNA in a quite diffusive manner which is much weaker than that of a Mg^{2+}-bridge[46]). Obviously, the abundant Mg^{2+}-bridges do not play an important role in the bound state of Z-DNA case. Z-DNA itself, like the specific properties of the contact surface, should be more responsible for the strong attraction between them.

3.5 Contact surface between two DNA

It is interesting to examine the composites of the contact surface between two DNA, and quantitatively measure the contributions from the hydrophilic and hydrophobic compo-

Table 1 Atoms with surface area > 0.1 nm^2, the surface area values are shown in the brackets

		Phosphate	Sugar	Base
AT-BDNA	A	O1P(0.32), O2P(0.29)	C4′(0.15), C5′(0.23)	–
	T	O1P(0.32), O2P(0.30)	C4′(0.13), C5′(0.23)	C7(0.40)
GC-BDNA	G	O1P(0.31), O2P(0.30)	C2′(0.11), C4′(0.13), C5′(0.23)	C8(0.11)
	C	O1P(0.30), O2P(0.31)	C4′(0.13), C5′(0.23)	C5(0.16)
GC-ZDNA	G	O1P(0.31), O2P(0.32)	C1′(0.14), C2′(0.18), C4′(0.12), C5′(0.11)	O6(0.13), N7(0.13), C8(0.31)
	C	O1P(0.25), O2P(0.30)	C5′(0.12)	–

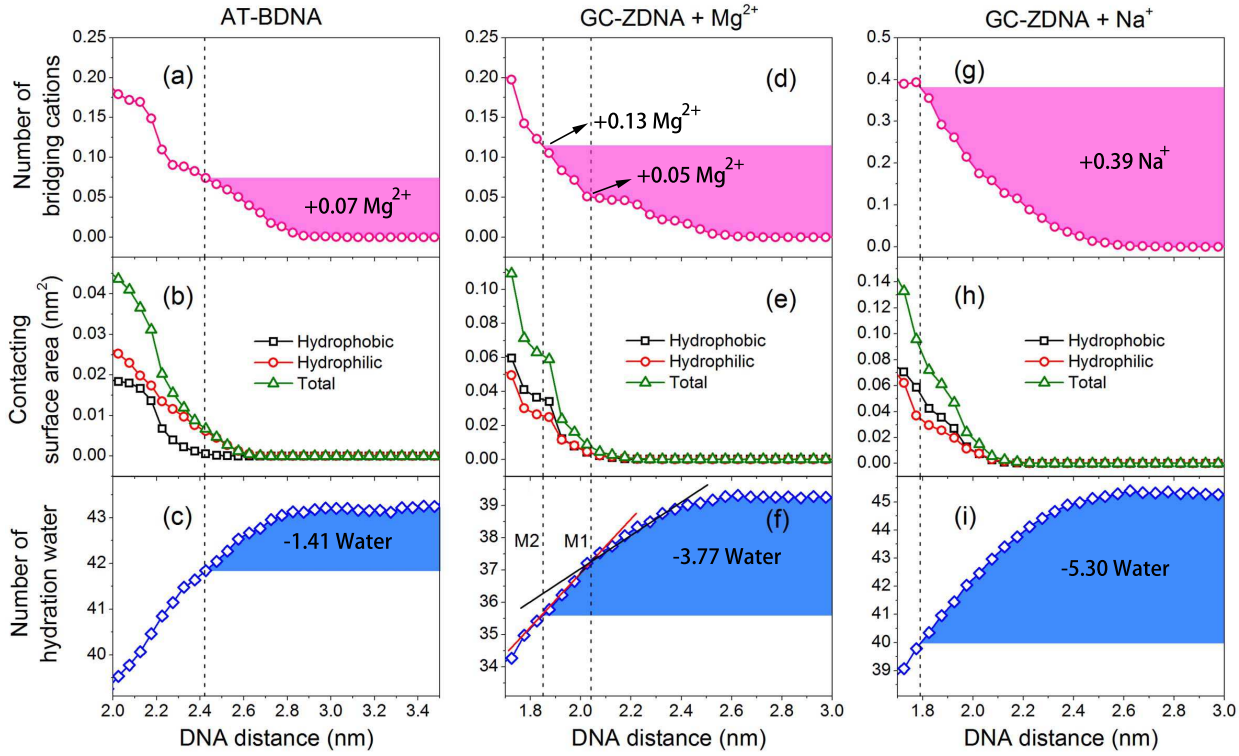

Fig. 5 The number of bridging cations, contact surface area and number of hydration water of **(a, b, c)** AT-BDNA with Mg^{2+}, **(d, e, f)** GC-ZDNA with Mg^{2+} and **(g, h, i)** GC-ZDNA with Na^{+} with respect to inter-DNA distance. The dash vertical lines indicate the inter-DNA distance of bound states. The red and black lines in Fig. **(f)** illustrate the slope of the water loss when approaching the bound states. Numbers of cation-bridges and water loss due to DNA contacting are highlighted as shaded areas and the corresponding values are also given.

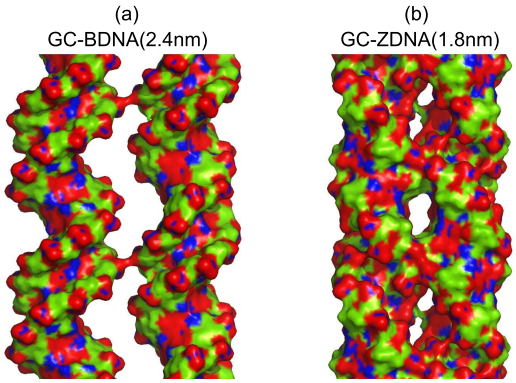

Fig. 6 Snapshots of two DNA at stable bound state: **(a)** GC-BDNA at 2.4 nm; **(b)** GC-ZDNA at 1.8 nm. DNA molecules are represented by a surface diagram. The color scheme is: green for hydrophobic (absolute value of atom charge is less than 0.2), red for negative hydrophilic (atom charge is less than -0.2), blue for positive hydrophilic (atom charge is larger than 0.2).

nents. We have classified the atoms on DNA surface into three categories according to their atomic charges: (1) hydrophobic, $|Q| \leq 0.2$; (2) negatively hydrophilic, $Q < -0.2$; (3) positively hydrophilic, $Q > 0.2$. The representative surfaces are shown in Fig. 6. It is clear that the outermost surface of B-DNA is mostly negatively hydrophilic, which consists of phosphate oxygen atoms. In contrast, for Z-DNA, apart from the negatively hydrophilic surface, hydrophobic sugar rings are also exposed. The outermost surface of Z-DNA has an alternative negatively hydrophilic-hydrophobic pattern.

The values of contact surface area (normalized to *bp*) are shown in Fig. 5(b, e, h). For B-DNA, the bound state at 2.41 nm has negligible contact area, 0.0083 nm^2 per *bp*. Meanwhile, hydrophilic surface completely dominates the contact area. For the local bound state of Z-DNA at M1, the contact surface is only 0.0081 nm^2 per *bp*, which is shared by hydrophilic and hydrophobic surfaces equally. The small values of contact area reflect that these bound states are water/ion-mediated.

For the case of Z-DNA at the close bound state of M2, the two Z-DNA have significantly larger contact surface area of 0.063 nm^2 per *bp*. This large value indicates that two DNA have formed tight contacts as shown in Fig. 6(b). It needs to be emphasized that the composites of the contact surface are different from those of B-DNA, which are 59% hydrophobic and 41% hydrophilic. Similiar trend is found for Na^+-mediated Z-DNA interactions as shown in Fig. 5(h).

3.6 DNA dewetting

During the binding process, the formation of hydrophobic contact surfaces revealed from the above analysis is accompanied by a nanoscale dewetting transition, where the interface water molecules are expelled into the bulk fluid and the interfacial region dewets (desolvates). This hydrophobic interaction is similar to the hydrophobic collapse in many other biomolecular self-assemblies, such as cell membrane formation and protein folding, where many recent studies[61–65] have shown that nanoscale dewetting (or dehydration) can provide significant driving forces for the collapse speed and system stability.

The dewetting process can be monitored by calculating the number of water molecules in the hydration shell during DNA binding. These water have been demonstrated to play a dominant role in the hydration thermodynamics[66,67]. In our calculation, the hydration shell is defined as the water molecules located within 0.5 nm to DNA surface. The values are summarized in Fig. 5(c, f, i).

For AT-BDNA, when the inter-DNA distance decreases from 3.5 nm to 2.41 nm (the global minimum), the hydration shell decreases from 43.26 to 41.85 H_2O per *bp*. The binding results in a loss of 1.41 water per *bp*. In comparison, a stronger dewetting happens for the case of GC-ZDNA. In Mg^{2+} electrolyte, the hydration shell decreases from 39.30 at 3.5 nm to 35.53 H_2O at 1.85 nm (the global minimum), resulting in a water number loss of 3.77 per *bp* as illustrated in Fig. 5(f). Moreover, the fitting slope of the number of hydration water profile approaching M2 state is sharper than that approaching M1 state, indicating a more dramatic dewetting process during the last binding stage. In the presence of Na^+, the binding of Z-DNA also results in a strong dewetting, with up to 5.30 water loss per *bp* as shown in Fig. 5(i). The different stability of the coordination water shell around Na^+/Mg^{2+} is responsible for the more pronounced water loss in the case of Na^+: Na^+ has a relatively loose and less stable coordination water shell than Mg^{2+}[46], so that the interfacial Na^+ ions will lose more coordinated water molecules during DNA binding. From this comparison, it is clear that the strong attraction between Z-DNA is reinforced by the strong dewetting effect of hydrophobic sugar rings which is consistent with the findings from contact surface analysis.

3.7 A two-stage process of Z-DNA binding

Combining the features of PMF, contact surface and dewetting transition in Fig. 5 and their firm relation, a two-stage Z-DNA binding process is outlined:

(1) In the first stage (distance is larger than 1.91 nm, where the energy barrier exists), two Z-DNA approach each other because bridging Mg^{2+} has effectively "screened" the repulsive forces. In this stage, Z-DNA binding is water/Mg^{2+}-mediated with an attractive potential well of -0.71 kcal/mol. This value is only slightly larger than those of B-DNA ($<$ -0.62 kcal/mol). In general, a binding energy of roughly -0.7

kcal/mol maybe the best that the charge screening effect and Mg^{2+}-bridges can contribute to the DNA interaction, but it is too weak to induce DNA condensation.

(2) In the second stage (distance is smaller than 1.91 nm), two Z-DNA form tight hydrophobic contact, which is accompanied by a strong dewetting process. These result in a strong attractive potential well, up to -1.64 kcal/mol.

4 Conclusions

The effects of DNA conformation in DNA interactions are studied with molecular dynamics simulations and free energy profiling methods. The contributions from cations, including both charge screening effect and cation-bridges, to DNA-DNA attraction are usually weak, with an attractive energy hardly exceeding -0.7 kcal/mol, which is not expected to be sufficient to induce DNA condensation. When DNA adopts the Z-form, part of the sugar rings expose to the solvent, making Z-DNA more hydrophobic. The direct hydrophobic contact of these sugar rings and dewetting effect can significantly enhance the inter – Z-DNA attraction.

The disclosure of the hydrophobic nature in Z-DNA interaction from current study may help to understand the specific and strong $Z\alpha$ – Z-DNA binding process in gene transcription. We believe our present studies can shed light on and stimulate more studies of the structure-function relationship of Z-DNA.

5 Acknowledgement

This work was partially supported by NTU Tier 1 grant RG 23/11, the National Natural Science Foundation of China (grant no. 11304214). R.Z. acknowledges support from the IBM Blue Gene Science Program.

References

1 N. Korolev, A. Allahverdi, A. P. Lyubartsev and L. Nordenskiöld, *Soft Matter*, 2012, **8**, 9322–9333.
2 D. C. Rau and V. A. Parsegian, *Biophysical Journal*, 1992, **61**, 260–271.
3 Y. Bai, R. Das, I. S. Millett, D. Herschlag and S. Doniach, *Proceedings of the National Academy of Sciences*, 2005, **102**, 1035–1040.
4 X. Qiu, K. Andresen, L. W. Kwok, J. S. Lamb, H. Y. Park and L. Pollack, *Physical Review Letters*, 2007, **99**, 038104.
5 R. W. Wilson and V. A. Bloomfield, *Biochemistry*, 1979, **18**, 2192–2196.
6 L. C. Gosule and J. A. Schellman, *Nature*, 1976, **259**, 333–335.
7 N. Korolev, N. V. Berezhnoy, K. D. Eom, J. P. Tam and L. Nordenskiöld, *Nucleic Acids Research*, 2009, **37**, 7137–7150.
8 J. C. Sitko, E. M. Mateescu and H. G. Hansma, *Biophysical Journal*, 2003, **84**, 419–431.
9 J. K. Choi, G. Sargsyan, M. Shabbir-Hussain, A. E. Holmes and M. Balaz, *The Journal of Physical Chemistry B*, 2011, **115**, 10182–10188.
10 I. Rouzina and V. A. Bloomfield, *The Journal of Physical Chemistry*, 1996, **100**, 9977–9989.
11 A. A. Kornyshev and S. Leikin, *The Journal of Chemical Physics*, 1997, **107**, 3656–3674.
12 N. Grønbech-Jensen, R. J. Mashl, R. F. Bruinsma and W. M. Gelbart, *Physical Review Letters*, 1997, **78**, 2477–2480.
13 B. I. Shklovskii, *Physical Review Letters*, 1999, **82**, 3268–3271.
14 E. Allahyarov, G. Gompper and H. Löwen, *Physical Review E*, 2004, **69**, 041904.
15 Z. Tan and S. Chen, *Biophysical Journal*, 2006, **91**, 518–536.
16 B. Luan and A. Aksimentiev, *Journal of the American Chemical Society*, 2008, **130**, 15754–15755.
17 N. Korolev, A. P. Lyubartsev and L. Nordenskiöld, *Advances in Colloid and Interface Science*, 2010, **158**, 32–47.
18 M. Behe and G. Felsenfeld, *Proceedings of the National Academy of Sciences*, 1981, **78**, 1619–1623.
19 T. J. Thomas and V. A. Bloomfield, *Biochemistry*, 1985, **24**, 713–719.
20 J. B. Chaires and M. T. Norcum, *Journal of Biomolecular Structure and Dynamics*, 1988, **5**, 1187–1207.
21 C. Ma, L. Sun and V. A. Bloomfield, *Biochemistry*, 1995, **34**, 3521–3528.
22 A. H. J. Wang, G. J. Quigley, F. J. Kolpak, J. L. Crawford, J. H. van Boom, G. van der Marel and A. Rich, *Nature*, 1979, **282**, 680–686.
23 S. C. Ha, K. Lowenhaupt, A. Rich, Y. G. Kim and K. K. Kim, *Nature*, 2005, **437**, 1183–1186.
24 A. Rich and S. Zhang, *Nature Reviews Genetics*, 2003, **4**, 566–572.
25 A. Herbert, J. Alfken, Y.-G. Kim, I. S. Mian, K. Nishikura and A. Rich, *Proceedings of the National Academy of Sciences*, 1997, **94**, 8421–8426.
26 A. Herbert, M. Schade, K. Lowenhaupt, J. Alfken, T. Schwartz, L. S. Shlyakhtenko, Y. L. Lyubchenko and A. Rich, *Nucleic Acids Research*, 1998, **26**, 3486–3493.
27 T. Schwartz, M. A. Rould, K. Lowenhaupt, A. Herbert and A. Rich, *Science*, 1999, **284**, 1841–1845.
28 M. Schade, C. J. Turner, R. Kühne, P. Schmieder, K. Lowenhaupt, A. Herbert, A. Rich and H. Oschkinat, *Proceedings of the National Academy of Sciences*, 1999, **96**, 12465–12470.
29 Y. G. Kim, K. Lowenhaupt, S. Maas, A. Herbert, T. Schwartz and A. Rich, *Journal of Biological Chemistry*, 2000, **275**, 26828–26833.
30 A. Rahmouni and R. Wells, *Science*, 1989, **246**, 358–363.
31 S. Lukomski and R. D. Wells, *Proceedings of the National Academy of Sciences*, 1994, **91**, 9980–9984.
32 G. P. Schroth, P. J. Chou and P. S. Ho, *Journal of Biological Chemistry*, 1992, **267**, 11846–11855.
33 P. C. Champ, S. Maurice, J. M. Vargason, T. Camp and P. S. Ho, *Nucleic Acids Research*, 2004, **32**, 6501–6510.
34 B. Wittig, S. Wölfl, T. Dorbic, W. Vahrson and A. Rich, *The EMBO journal*, 1992, **11**, 4653.
35 S. Wölfl, C. Martinez, A. Rich and J. A. Majzoub, *Proceedings of the National Academy of Sciences*, 1996, **93**, 3664–3668.
36 S. Wölfl, B. Wittig, T. Dorbic and A. Rich, *Biochimica et Biophysica Acta (BBA)-Gene Structure and Expression*, 1997, **1352**, 213–221.
37 J. V. Ditlevson, S. Tornaletti, B. P. Belotserkovskii, V. Teijeiro, G. Wang, K. M. Vasquez and P. C. Hanawalt, *Nucleic Acids Research*, 2008, **36**, 3163–3170.
38 S. Feng, H. Li, J. Zhao, K. Pervushin, K. Lowenhaupt, T. U. Schwartz and D. Peter, *Nature Structural & Molecular Biology*, 2011, **18**, 169–176.
39 L. Dai, Y. Mu, L. Nordenskiöld and J. R. C. van der Maarel, *Physical Review Letters*, 2008, **100**, 118301.
40 C. Maffeo, B. Luan and A. Aksimentiev, *Nucleic acids research*, 2012, **40**, 3812–3821.
41 P. Várnai and Y. Timsit, *Nucleic acids research*, 2010, **38**, 4163–4172.
42 H. Li, J. Xiao, J. Li, L. Lu, S. Feng and P. Dröge, *Nucleic Acids Research*, 2009, **37**, 2737–2746.
43 K. Brzezinski, A. Brzuszkiewicz, M. Dauter, M. Kubicki, M. Jaskolski and Z. Dauter, *Nucleic Acids Research*, 2011, **39**, 6238–6248.
44 D. Studio, *Accelrys Inc.: San Diego, CA, USA*, 2009.
45 A. D. MacKerell, D. Bashford, Bellott, R. L. Dunbrack, J. D. Evanseck,

M. J. Field, S. Fischer, J. Gao, H. Guo, S. Ha, et and al., *J. Phys. Chem. B*, 1998, **102**, 3586–3616.
46 W. Li, L. Nordenskiöld and Y. Mu, *The Journal of Physical Chemistry B*, 2011, **115**, 14713–14720.
47 D. Van Der Spoel, E. Lindahl, B. Hess, G. Groenhof, A. E. Mark and H. J. Berendsen, *Journal of computational chemistry*, 2005, **26**, 1701–1718.
48 A. Pérez, I. Marchán, D. Svozil, J. Sponer, T. E. Cheatham, C. A. Laughton and M. Orozco, *Biophysical Journal*, 2007, **92**, 3817–3829.
49 W. L. Jorgensen, J. Chandrasekhar, J. D. Madura, R. W. Impey and M. L. Klein, *Journal of Chemical Physics*, 1983, **79**, 926–935.
50 J. P. Ryckaert, G. Ciccotti and H. J. C. Berendsen, *Journal of Computational Physics*, 1977, **23**, 327–341.
51 J. Yoo and A. Aksimentiev, *The Journal of Physical Chemistry Letters*, 2011, **3**, 45–50.
52 U. Essmann, L. Perera, M. L. Berkowitz, T. Darden, H. Lee and L. G. Pedersen, *Journal of Chemical Physics*, 1995, **103**, 8577–8593.
53 T. Darden, L. Perera, L. Li and L. Pedersen, *Structure*, 1999, **7**, 55–60.
54 G. M. Torrie and J. P. Valleau, *Chemical Physics Letters*, 1974, **28**, 578–581.
55 J. S. Hub, B. L. de Groot and D. van der Spoel, *Journal of Chemical Theory and Computation*, 2010, **6**, 3713–3720.
56 V. A. Bloomfield, *Current opinion in structural biology*, 1996, **6**, 334–341.
57 R. R. Sinden, *DNA Structure and Function*, Gulf Professional Publishing, 1994.
58 T. Schoenknecht and H. Diebler, *Journal of Inorganic Biochemistry*, 1993, **50**, 283–298.
59 M. Guéron, J. P. Demaret and M. Filoche, *Biophysical Journal*, 2000, **78**, 1070–1083.
60 Y. Gao, M. Sriram and A. H. Wang, *Nucleic Acids Research*, 1993, **21**, 4093–4101.
61 P. Liu, X. Huang, R. Zhou and B. Berne, *Nature*, 2005, **437**, 159–162.
62 R. Zhou, X. Huang, C. J. Margulis and B. J. Berne, *Science*, 2004, **305**, 1605–1609.
63 T. Young, L. Hua, X. Huang, R. Abel, R. Friesner and B. Berne, *Proteins: Structure, Function, and Bioinformatics*, 2010, **78**, 1856–1869.
64 B. J. Berne, J. D. Weeks and R. Zhou, *Annual Review of Physical Chemistry*, 2009, **60**, 85–103.
65 Y. Wu, R. Vadrevu, S. Kathuria, X. Yang and C. R. Matthews, *Journal of Molecular Biology*, 2007, **366**, 1624–1638.
66 W. Li and Y. Mu, *The Journal of Chemical Physics*, 2011, **135**, 134502.
67 W. Li, R. Zhou and Y. Mu, *The Journal of Physical Chemistry B*, 2012, **116**, 1446–1451.